

Article

Research on an Axial Flux PMSM with Radially Sliding Permanent Magnets

Jing Zhao ^{1,2}, Bin Li ^{1,*} and Zhongxin Gu ¹

¹ School of Automation, Beijing Institute of Technology, Beijing 100081, China;
E-Mails: zhaojing_bit@bit.edu.cn (J.Z.); bitzhongxingu@gmail.com (Z.G.)

² School of Electrical Engineering and Automation, Harbin Institute of Technology,
Harbin 150080, China

* Author to whom correspondence should be addressed; E-Mail: libin_hit@hotmail.com;
Tel./Fax: +86-10-6891-2460.

Academic Editor: Omar Hegazy

Received: 26 December 2014 / Accepted: 15 February 2015 / Published: 27 February 2015

Abstract: Axial flux permanent-magnet synchronous machines (PMSMs) are very suitable candidates for the power train of electric vehicles (EVs) due to high power density and high efficiency. This paper researches an axial flux PMSM with radially sliding permanent magnets (PMs) to fulfill field-weakening control. The field weakening principle and the structure of this kind of axial flux PMSM by mechanical method of sliding PMs are proposed and analyzed. The influences of radially sliding PMs on magnetic flux density distribution, inductance, flux linkage and torque are analyzed and discussed based on 3D finite element method (FEM). The field weakening capabilities by mechanical method and electrical method are compared. The field weakening capability of the machine can be much improved by the optimized combination of the two methods, which is very satisfying for EV drive application. The forces on the PMs are analyzed and calculated. The hysteretic characteristics caused by the friction of the PMs are investigated, which provide useful reference for designing this kind of machine.

Keywords: axial flux; permanent magnet synchronous machine (PMSM); sliding permanent magnets; field weakening; inductance; hysteretic characteristic

1. Introduction

With the problems of air pollution and energy consumption getting more and more concerns, the traditional vehicles with internal combustion engine (ICE) will be probably eliminated in future transportation because they consume fuel derived from non-renewable resources and release exhaust gas. However, electric vehicles (EVs) are rapidly developed during recent decades due to the advantages of energy-saving, non-emission and low noise pollution [1,2]. EVs have the potential to provide a perfect solution to energy security and environmental impacts in the future. Especially, if they can be powered by electrical energy generated from renewable sources, such as wind, solar, *etc.*, they will not need extra petroleum.

As the key part of EVs, different types of traction machines are tried to be used in EVs [3–8]. Axial flux permanent-magnet synchronous machines (PMSMs) are becoming more and more attractive in many propulsion applications due to the advantages of high efficiency, power factor and power density [9–16]. Undoubtedly, they are also very suitable to propel EVs [17–19]. When the axial-flux PMSM drives the EV, it requires a higher torque at low speed and a lower torque at high speed, which implies that the axial-flux PMSM needs a fairly wide field weakening range.

When the PMSM operates normally, neglecting the little voltage on the armature resistance, the voltage Equation of the PMSM can be expressed as [20]

$$u_{\text{lim}} = \omega \sqrt{(L_q i_q)^2 + (L_d i_d + \psi_f)^2} \quad (1)$$

where u_{lim} is the supplied limit voltage, ω is the electrical speed, L_d and L_q are the d - and q -axis inductances, i_d and i_q are the d - and q -axis current, ψ_f is the flux linkage produced by PM.

Constant torque control is adopted below base speed and the voltage will increase with the speed increasing. However, field weakening is needed above base speed where the back electromotive force (EMF) equals the supplied limit voltage. As for normal PMSM, ψ_f produced by PM is fixed. Thus, based on Equation (1), traditional electrical method, i.e. increasing the d -axis demagnetizing current and decreasing the q -axis current, is usually adopted to improve the operating speed range for PMSM.

However, because of the disk structure of axial flux PMSM, most axial flux machines adopt surface-mounted permanent magnets (PMs) and have large air gaps, which result in small d - and q -axis inductances. This makes the field weakening more difficult to execute for wide range operation by using traditional electrical methods.

In order to improve the wide speed range of axial flux PMSM, various special field-weakening methods are proposed and researched [21–30]. In [21], the rotor pole of the machine adopts a combination of a rare earth magnet (neodymium–iron–bore) and soft laminated iron to reduce the total d -axis reluctance. So the field-weakening characteristic is obtained by injecting a relatively small negative d -axis current. The axial flux PM machine in [22] adopts fractional-slot winding and additional cores enclosing end windings to increase the inductance and then the field weakening capability. In [23,24], a hybrid dual-rotor–single-stator axial machine with a DC field coil located on the stator and a rotor made of alternate PMs and iron teeth is proposed to fulfill a reasonable range of field weakening. This technique allows an easy control of the axial gap flux with DC field current but without any negative effects of current injection. In addition, mechanical methods of adjusting the air-gap field are also popular in axial flux PM machine. In [25], an axial-flux permanent magnet (AFPM) machine with two

rotors and one stator regulates the flux linkage through displacement of the two rotors by mechanical solutions. Constant power generation is thus achieved with very inexpensive devices. Changing the air gap of the axial flux PM machine by mechanical method is another way to fulfill the field weakening [26–28]. Early in 2001, [29] proposed an axial flux PM machine with radially movable PMs to weaken the air gap flux. But there was no theoretical research results showing the effect of this structure. Considering the speed requirement for the machine used for EVs, the axial flux PMSM with radially sliding PMs adopting mechanical device similar to the structure described in [29] will be investigated comprehensively in this paper.

Firstly, the field weakening principle and the structure of this kind of axial flux PMSM with radially sliding PMs are introduced and analyzed. Secondly, the influences of radially sliding PMs on magnetic characteristics are analyzed and discussed based on 3D finite element method (FEM). Thirdly, the field weakening capabilities by the mechanical method and by electrical method are compared. At last, the forces on the PMs are researched and the hysteretic characteristics caused by the friction of the PMs are investigated.

2. Field Weakening Principle of the Axial Flux PMSM with Radially Sliding PMs

As for normal PMSM, when the rotor is rotating, centrifugal force will be imposed on the PMs mounted on the rotor. The PMs on the rotor are usually fixed by glue, glass fiber tape or directly inserted inside the rotor to overcome the centrifugal force. During a constant speed, if the resultant force provided is smaller than the centrifugal force, the PMs will run away from the circle center. In this paper, centrifugal movement of the PMs will be utilized to make the PMs radially slide away from the circle center when the speed is higher than the base speed. The schematic diagram of the field weakening principle using radially sliding PMs is shown in Figure 1.

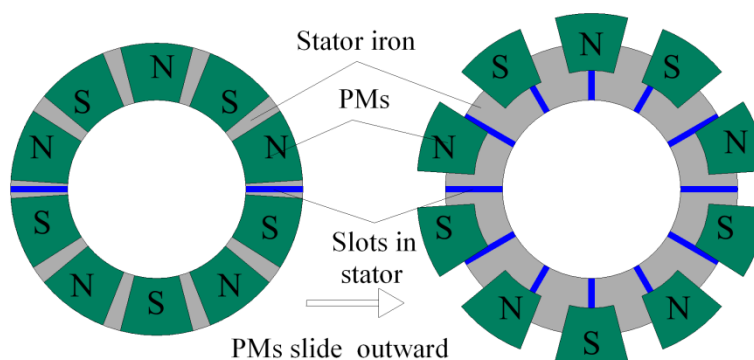


Figure 1. Schematic diagram of the field weakening principle using radially sliding permanent magnets (PMs).

When the speed is below the base speed, the PMs stay at the initial position, where the PMs face stator iron directly. When the speed increases to base speed, the PMs are designed to start sliding outward under the centrifugal force. Then the area of PMs facing stator iron decreases. In this case, the main flux produced by the PMs can be expressed as

$$\Phi_{\delta} = \frac{b_m B_r A_{meq}}{\sigma} \quad (2)$$

where b_m is the working point of permanent magnet, B_r is the remnant flux density, A_{meq} is the equivalent area under each pole, σ is the flux leakage coefficient.

The flux linkage ψ_f produced by PM can be expressed as

$$\psi_f = N \cdot k_{w1} \cdot \Phi_\delta = N \cdot k_{w1} \cdot \frac{b_m B_r A_{meq}}{\sigma} \quad (3)$$

where N is the turns-in-series per phase of the armature winding, k_{w1} is the fundamental winding factor.

Due to the decrease of A_{meq} , the flux linkage ψ_f will also decrease. Based on Equation (1), when the limit voltage u_{lim} of the machine is fixed, the speed ω will increase consequentially with flux linkage reducing. This is the field weakening principle using the mechanical method without current adjustment.

3. Structure of the Axial Flux PMSM with Radially Sliding PMs

The axial flux PMSM with radially sliding PMs in this paper contains two electromagnetic parts: a conventional disk stator with three-phase windings and a novel disk rotor with radially sliding PMs. The structure of the rotor is much improved to realize the field weakening by moving the sliding PMs in radial direction. As shown in Figure 2, the novel rotor consists of the rotor core, the sliding PMs, the PM carriers where the PMs are embedded in, the slideways on which the PMs slide, and the spring device to provide the main centripetal force. The main differences between the novel rotor structure and the traditional rotor structure are as follows:

(1) The outer diameter of the new rotor is bigger than that of the traditional rotor. The traditional outer diameter is the same with the PMs outer diameter, while the new outer diameter should be bigger to provide the space for the PMs sliding. In addition, there is an end frame to limit the maximal sliding distance of the PMs.

(2) In order to connect PM with the spring device, PM carriers with spring connecting end are needed to carry the PMs.

(3) Slideways are needed to avoid the PMs diverging from the original radial line under the centrifugal force. The slideway is along with the radial line. The PM is fixed on the slider inside the slideway.

(4) The springs are necessary to provide the main centripetal force when the PMs are rotating. The springs have initial tension load to overcome the centrifugal force under the base speed, because the PMs should not slide under the base speed.

Because the novel rotor has the sliding PMs in radial direction, little field weakening current is needed. And there is almost no risk of demagnetization of the PMs. The field weakening range can be realized by changing the slide distance of the PMs, which raises the potential of the field weakening to a very high level. But what should be noted is that: due to the sliding friction, the radial displacement of the PMs may not be the same for all the PMs in actual operation, which could cause voltage dissymmetry, circulating currents between parallel paths, and bending torque. This risk should be avoided as possible in manufacture. The performances researched in this paper are based on the ideal situations.

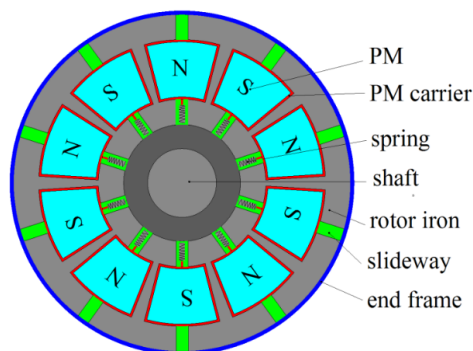


Figure 2. Schematic diagram of the novel rotor with sliding PMs.

4. Investigation of the Electromagnetic Characteristics

When the machine speed is above the base speed, the centrifugal force becomes bigger than the initial tension load of the springs, which makes the PMs slide in radial direction. The area where the PMs face the stator core will change, which will affect the magnetic field distribution and the electromagnetic performances. In this section the influences of the sliding PMs on the electromagnetic characteristics will be analyzed on the aspects of magnetic field distribution, inductance, magnetic flux linkage of windings and torque. All of these aspects are related to the position of the PMs, but not related to the speed of the machine. The main parameters of the axial flux PMSM investigated are shown in Table 1. The half and whole 3D FEM models both are adopted in this following simulation. When the performance is calculated in magnetostatic case, such as distribution of field flux density, the whole 3D-FEM model is adopted. When the performance is calculated in transient case, such as torque, the half 3D-FEM model is adopted. The half 3D-FEM model of the axial flux PM machine with PMs sliding outward is shown in Figure 3. Considering that the effect of slideways and spring is too weak on electromagnetic performance, the slideways are neglected in the 3D FEM model in order to simplify the model and reduce the mesh numbers. Figure 4 is the cross diagram of radial section of the axial flux PMSM when PMs slide outward. When the PMs slide outward, the machine can be divided into three sections in the radial direction, as shown in Figure 4. Part I contains stator iron and rotor iron but no PMs. Part II contains stator iron, rotor iron and PMs. Part III contains rotor iron and PMs but no stator iron.

Table 1. Main initial parameters of axial flux PMSM with radially sliding permanent magnets (PMs).

Symbol	Machine Parameter	Values	Unit
D_{PMi}	Inner diameter of PM	75	mm
D_{PMo}	Outer diameter of PM	123	mm
D_{si}	Inner diameter of stator iron	75	mm
D_{so}	Outer diameter of stator iron	123	mm
D_{ro}	Outer diameter of rotor iron	158	mm
d	Maximal sliding distance	33	mm
n_r	Base speed	3000	rpm
T_{ra}	Rated output torque	32	Nm
U_{limit}	Voltage	110	V

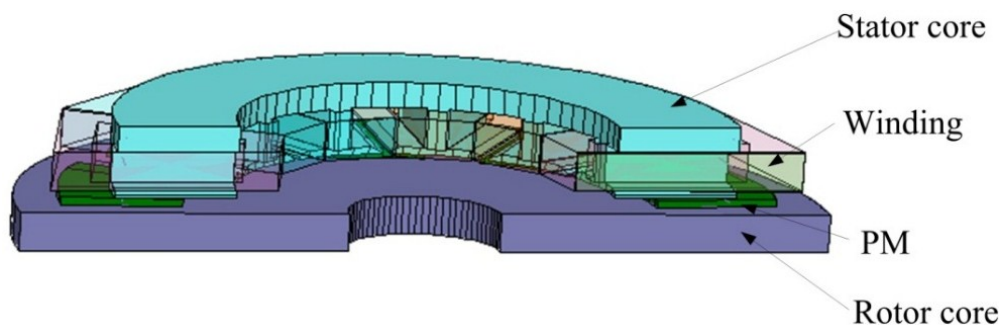


Figure 3. Half 3D finite-element-method (3D-FEM) model of the axial flux PM machine with PMs sliding outward.

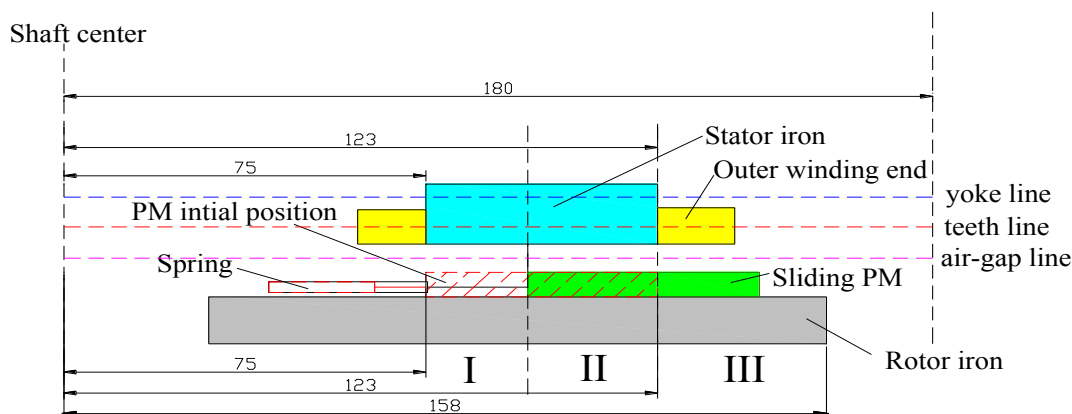


Figure 4. Cross diagram of radial section of the axial flux permanent-magnet synchronous machine (PMSM) when PMs slide outwards.

4.1. Influences on the Magnetic Flux Density Distribution

Two kinds of stator meeting the 3D flux characteristics of the axial flux PMSM are compared in this part. One is the stator core with rolled lamination, which can be made with long sheet of steel rolled up and slots cut during the rolling [31], as illustrated in Figure 5. In this case, it is easy for the magnetic flux to pass the stator core steel along the axial and circumferential direction. However, it is hard to pass the stator core along radial direction, which is perpendicular to the laminated steel. The other stator is made of soft magnetic composite (SMC). The SMC is made from powder iron material and can be molded to any shape theoretically with a similar process to plastic injection molding [32,33]. The stator core with SMC has equal magnetic permeability in every direction. Due to different processing methods, the magnetic flux density distributions of the machines with the two different materials may be different and compared in this part. Considering that the changing law of the flux linkage, inductance and torque will not be influenced by material, only the performances of the machine with SMC are presented in following parts.

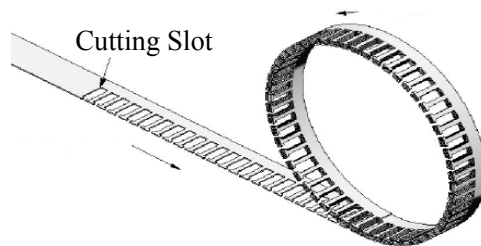


Figure 5. Scheme of rolled lamination [31].

The amplitude of magnetic flux density distributed in the air gap, teeth and yoke of the two machines with rolled lamination stator and SMC stator are shown in Figures 6–8. The magnetic density distributions in the air gaps of the two machines are almost the same. The distribution laws of flux density in teeth and yoke in machine with rolled laminated stator are the same as in the air gaps, because it is hard for the flux in laminated stator to pass the stator core along radial direction as mentioned above and shown as in Figure 9. The flux density in Part I is almost reduced to zero without PMs. Flux density in part II changes little due to the existence of the stator iron, rotor iron and PMs as normal axial flux PMSM. The flux produced by the PMs in area III is much reduced because the equivalent reluctance in this area becomes much bigger without the stator iron. However, the distribution laws of flux density in teeth and yoke in SMC stator are much different from that in laminated stator. Although the air-gap flux density in part I is much reduced, the flux density in part I will enter stator core. Due to the 3D permeability of SMC, the flux in teeth and yoke from part II will distribute all over of the SMC stator core, including the core in part I, as shown in Figure 10. So the magnetic flux density distribution in teeth and yoke of SMC stator are relatively even along the radial direction. However, with the PMs sliding outward, magnetic flux density distribution in teeth and yoke of SMC stator becomes small due to the reduction of part II area.

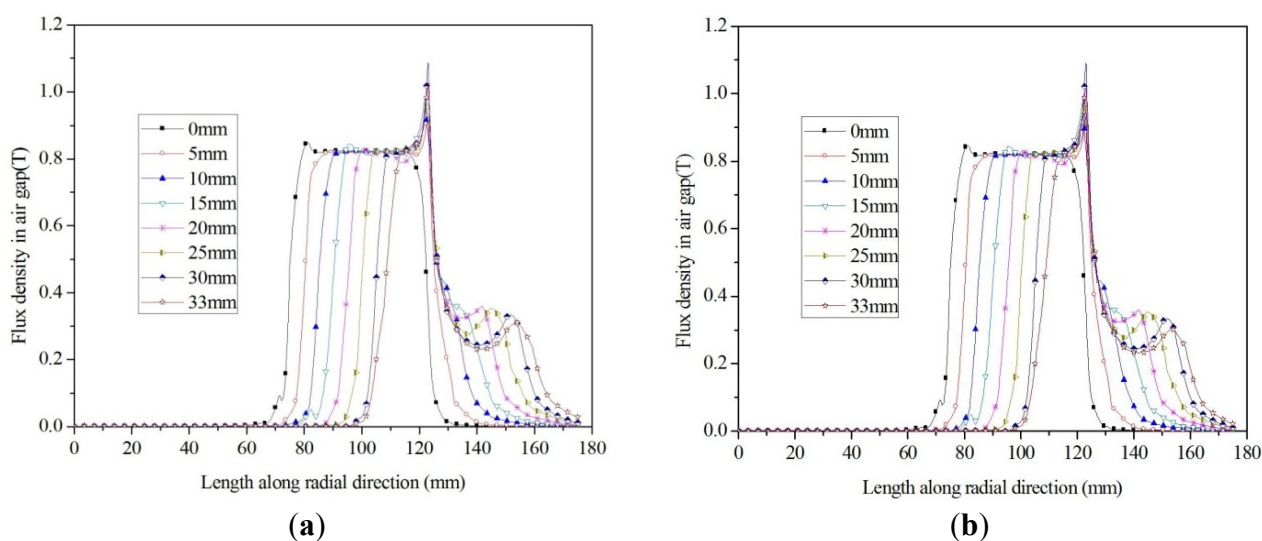


Figure 6. The magnetic flux density distributed in the air gap: (a) rolled lamination (b) soft magnetic composite (SMC).

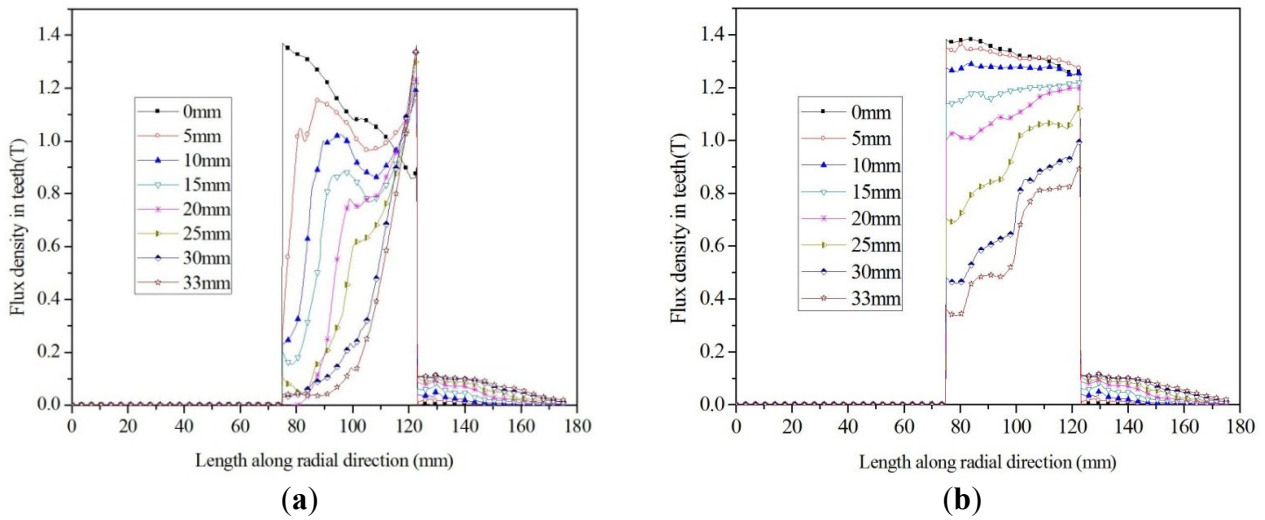


Figure 7. The magnetic flux density distributed in the teeth: (a) rolled lamination (b) SMC.

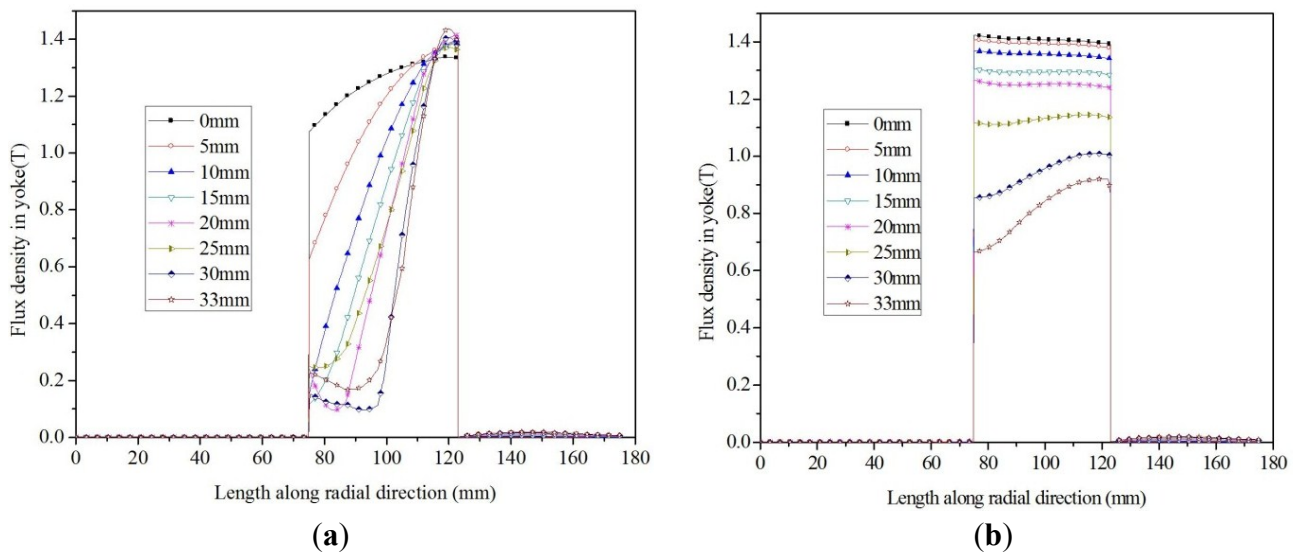


Figure 8. The magnetic flux density distributed in the yoke: (a) rolled lamination (b) SMC.

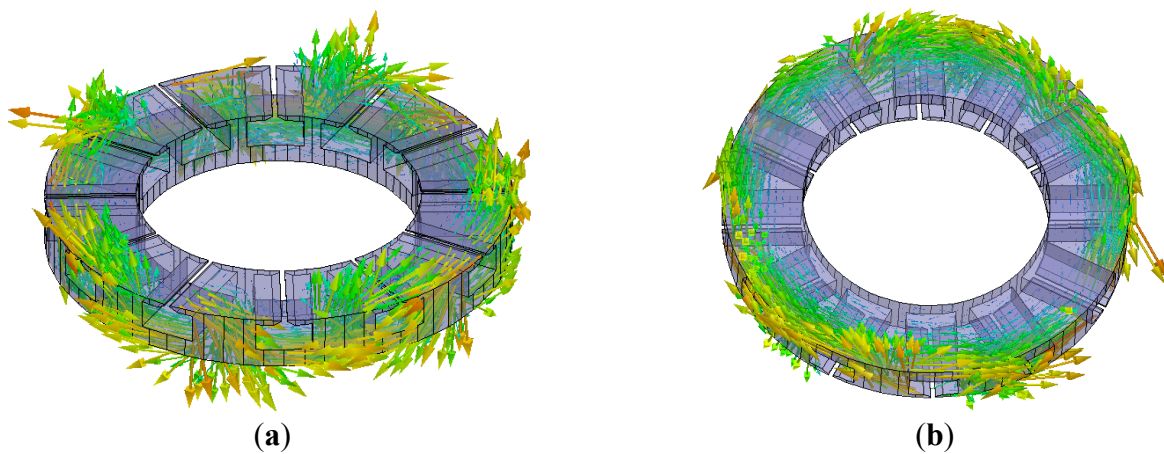


Figure 9. 3D distribution of magnetic flux density in the rolled laminated stator when PMs sliding outward: (a) view from teeth side, and (b) view from yoke side.

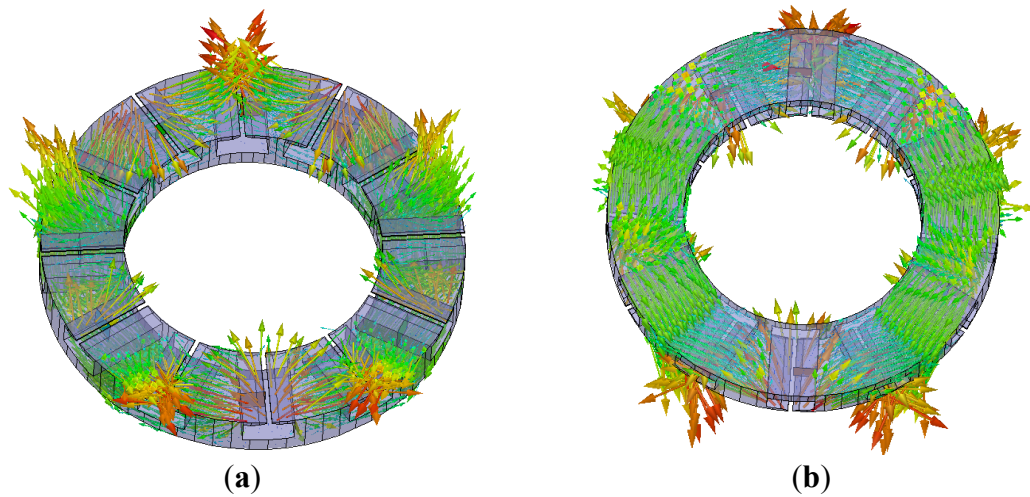


Figure 10. 3D distribution of magnetic flux density in the SMC stator when PMs sliding outward: (a) view from teeth side, and (b) view from yoke side.

4.2. Influences on the Inductances

According to Equation (1), the inductances will influence the field weakening range, so it is necessary to evaluate the influence of the radial sliding PMs on the *d*- and *q*-axis inductances.

As is known, the inductance of a circuit can be calculated by

$$L = \psi / i \tag{4}$$

where *L* is the inductance of the circuit, *i* is the current in the circuit, ψ is the flux linkage produced by *i*.

For a machine, the flux linkage generated by certain current can be influenced by the magnetic circuit structure, which can be expressed as

$$\psi \propto \Phi N \propto F_a \Lambda N \propto I N^2 \Lambda \tag{5}$$

where *I* is the armature current, F_a is the magnetomotive force (MMF) generated by armature, Φ is the flux per pole generated by F_a , and Λ is the permeance of the magnetic circuit.

In order to analyze the magnetic circuit about the armature MMF directly, the MMF of PM is not considered here. Then the magnetic circuit of the armature MMF can be illustrated in Figure 11. In Figure 11 Λ_{sy} , Λ_{st} is the yoke and teeth permeance of the stator core, respectively, Λ_{σ} is the leakage permeance, Λ_{δ} is the air gap permeance, and Λ_r is the rotor permeance. The total equivalent permeance Λ of the magnetic circuit can be deduced as

$$\Lambda = \frac{1}{\frac{1}{\Lambda_{sy}} + \frac{1}{\Lambda_{st}} + \frac{1}{\Lambda_{a\sigma} + \frac{\Lambda_r \Lambda_{\delta}}{\Lambda_r + \Lambda_{\delta}}}} \tag{6}$$

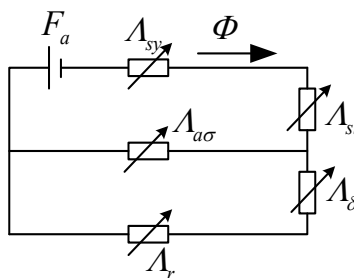


Figure 11. The equivalent magnetic circuit of the armature magnetomotive force (MMF).

When the PM slide outward, the saturation of the core will decrease based on Figures 7 and 8. A_{sy} , A_{st} and A_{σ} will increase accordingly. Even if the A_{δ} and A_r change little, the total equivalent permeance Λ will increase with the PM sliding out, which will result in the inductance increase. The d - and q -axis inductances are calculated by 3D FEM according to [34]

$$L_d = \left| \frac{\psi_f - \psi_d}{I_d} \right| \quad (7)$$

$$L_q = \frac{\psi_q}{I_q} \quad (8)$$

where L_d and L_q are d - and q -axis inductances, ψ_d and ψ_q are d - and q -axis flux linkage, I_d and I_q are d - and q -axis current.

For the same current, the changing laws of d - and q -axis inductances *versus* the sliding distance are shown in Figure 12. The simulated inductances are in accordance with the analysis. The d -axis and q -axis inductances increase rapidly at first and then slowly with the PMs sliding outward, which indicates that the saturation of the iron core has much influence on the inductance. In order to validate the effect of iron core saturation on the inductance, inductances in an unsaturated case are also calculated and shown in Figure 12. The relative permeability of iron core in unsaturated case is set to be very high $\mu_{\text{iron}} = 300000$ to be close to infinite iron core permeability. It can be seen from Figure 12, with the PMs sliding outward, the inductances in unsaturated case are almost unchanged due to a nearly constant equivalent permeance of the magnetic circuit. With the PMs sliding outward, the saturation in normal case decreasing to unsaturation, the inductances in normal case is close to inductances in unsaturated case, which validates that the saturation dose has much effect on the inductances of the machine with sliding PMs.

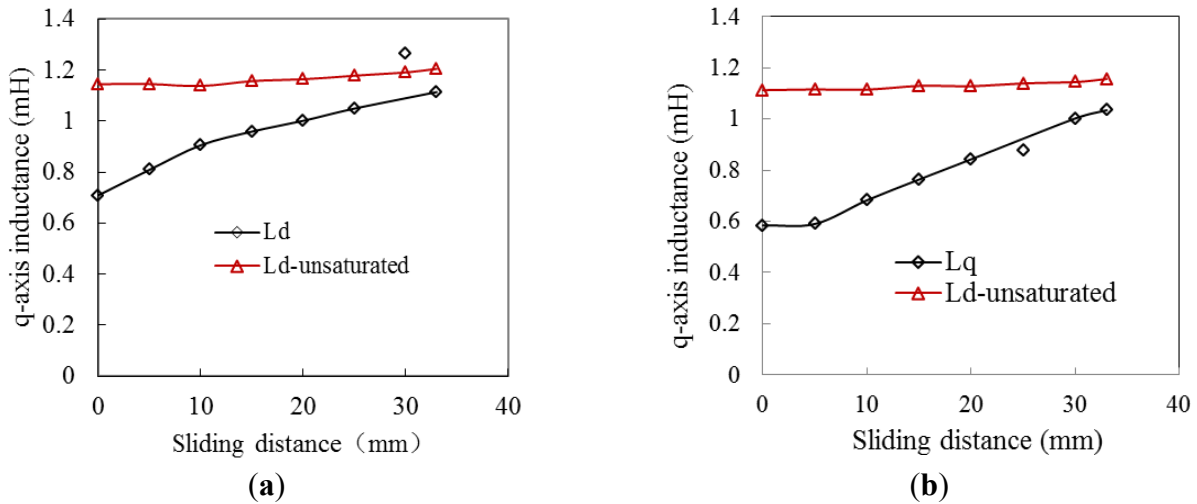


Figure 12. The *d*- and *q*-axis inductances versus the sliding distance of the PMs: (a) L_d and (b) L_q .

4.3. Influences on the Flux Linkage

When the principle of this machine is analyzed, it mentions that the flux linkage produced by PMs is reduced with the PMs sliding outward. In this section, the flux linkage at no load $\psi_{no-load}$ produced by PMs independently and the flux linkage at load ψ_{load} produced by PMs and armature current together will be calculated quantitatively by 3D FEM.

$$\psi_{load} = \sqrt{(L_q i_q)^2 + \psi_f^2} \tag{9}$$

Considering only adopting the mechanical method of field weakening by sliding PMs, the armature current is fixed and only has *q*-axis component when calculating ψ_{load} . The changing laws of $\psi_{no-load}$ and ψ_{load} with the PMs sliding distance are shown in Figure 13. It can be seen that the decreased ratio of $\psi_{no-load}$ and ψ_{load} are different. When the PMs slide outward to 33 mm, the $\psi_{no-load}$ is decreased to 48.5%, while the ψ_{load} is decreased to 66.4%. The field weakening effect at load is poorer than that at load, because the L_q increases during the PMs sliding process.

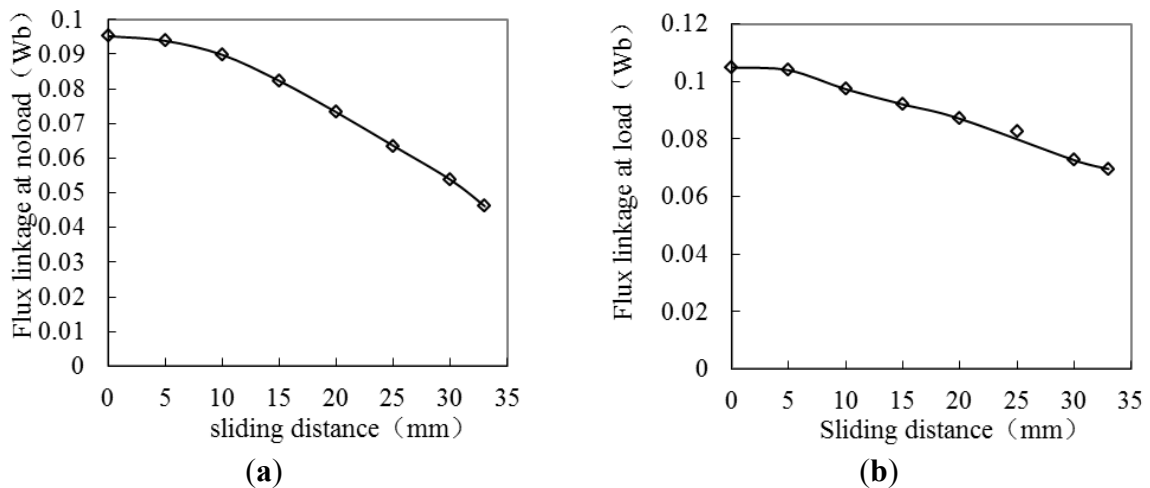


Figure 13. Changing law of flux linkage with the PMs sliding distance: (a) $\psi_{no-load}$ at no load (b) ψ_{load} at load.

4.4. Influences on the Torque

Because the PMs sliding has much influence on the distribution of the magnetic field, consequently, the electromagnetic torque must also be influenced. So the influence of the PMs sliding on torque is researched in this part. The electromagnetic torque T_{em} can be expressed as

$$T_{em} = p \left[\psi_f i_q + (L_d - L_q) i_d i_q \right] \quad (10)$$

where p is the number of pole pairs.

Under a certain i_q without i_d , the electromagnetic torque T_{em} of the machine is proportional to the ψ_f and T_{em} will decrease with the PMs sliding outward, which will be similar as the ψ_f . Using 3D FEM, the calculated average electromagnetic torque of the machine is shown in Figure 14. The calculated results are in agreement with the analysis.

The cogging torque is also influenced by sliding PMs. The calculated cogging torque of the machine is shown in Figure 15. In Figure 15a, only the cogging torque at sliding distances of 0 mm, 15 mm and 30 mm are shown to see the curves more clearly. Figure 15b shows the relationship between peak-peak value of cogging torque and the PM sliding distance. The cogging torque also decreases with the PMs sliding outward. In addition, due to the adoption of fractional slot and optimization of shape of PMs when designing the machine, the cogging torque is small.

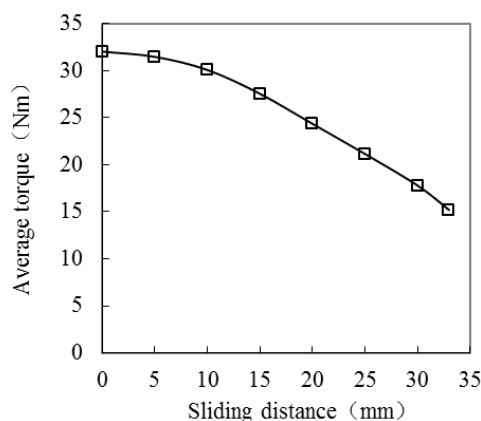


Figure 14. Average electromagnetic torque with the PMs sliding distance.

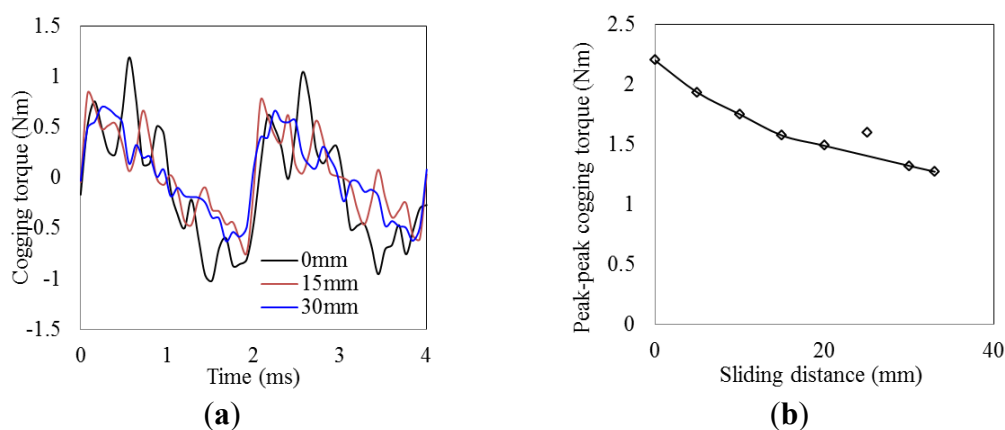


Figure 15. Cogging torque with the PMs sliding distance: (a) cogging torque curve, (b) peak-peak value of cogging torque.

5. Evaluation on the Field Weakening Characteristics

The field weakening characteristics can be expressed by torque-speed curve and power-speed curve. Constant torque area is below the base speed. Field weakening area is above the base speed, which is also constant power area ideally. During the constant torque area, a constant current is applied on q axis. Above the base speed, several cases are compared with the voltage no more than u_{lim} .

5.1. Comparison of Mechanical Method and Traditional Electrical Method

Traditional electrical method of increasing the i_d and decreasing i_q without moving the PMs is researched to provide the reference of evaluating the mechanical method. The torque-speed curve using traditional electrical method can be obtained by normal method. Mechanical method of sliding PMs is researched independently with a constant current on q axis. In this case, the relationship between the speed and the PM sliding distance can be obtained according to Equation (11) and Figure 13b indirectly, as shown in Figure 16. Then the torque-speed curve can be obtained based on Figures 14 and 16. The field weakening results of the electrical and mechanical methods are shown in Figure 17. It can be seen that the field weakening effect caused by mechanical method is almost the same as that by traditional electrical method. The speed is increased by no more than two times of the base speed using either of the two methods. The power cannot keep constant above the base speed. So the combination of the mechanical and electrical method is researched in the following part.

$$u_{lim} = \omega \sqrt{(L_q i_q)^2 + \psi_f^2} \quad (11)$$

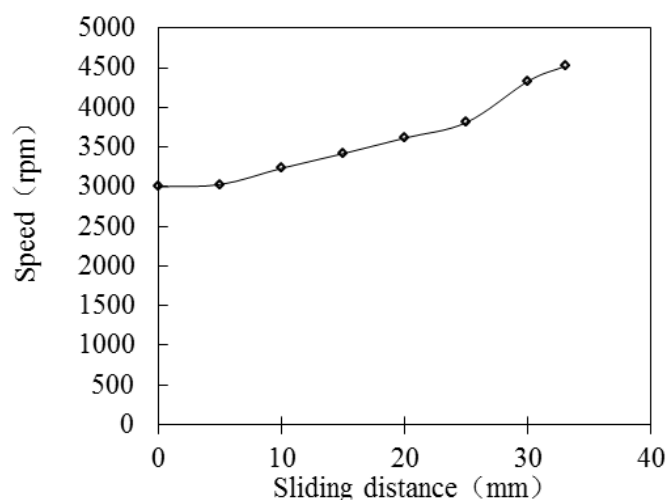


Figure 16. Relationship between the speed and the PMs sliding distance.

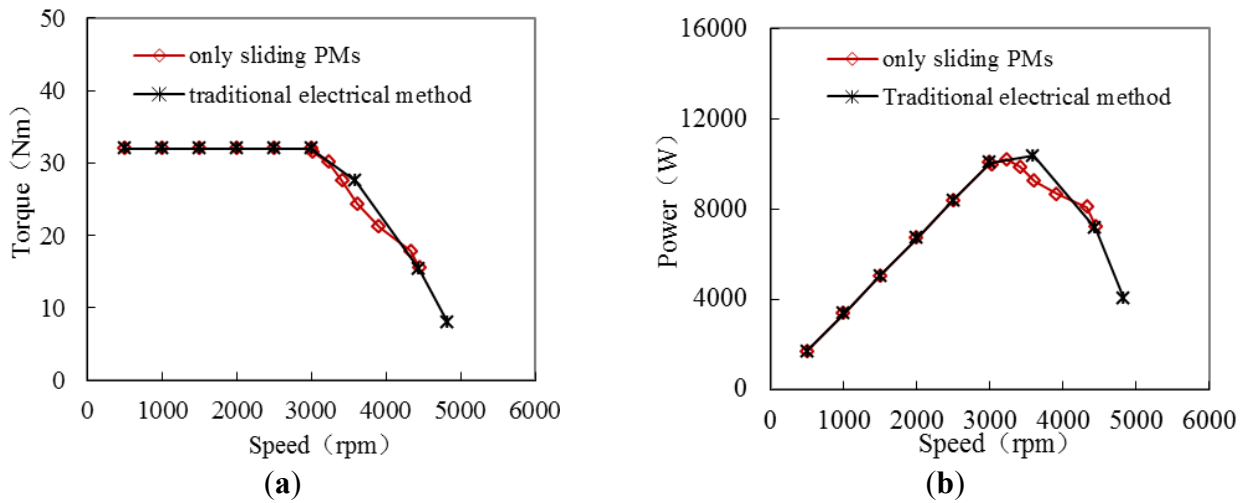


Figure 17. Comparison of the field weakening results by mechanical and electrical methods: (a) torque-speed and (b) power-speed.

5.2. Combination of Mechanical Method and Electrical Method

As analyzed before, field-weakening effect caused by only sliding the PMs is not satisfying due to the strong armature reaction at load. For a certain machine, the q -axis current can be reduced to decrease the flux linkage at load, thus enhancing the speed range. So the i_q is tried to be reduced without any i_d during the PMs sliding outward. The corresponding torque-speed and power-speed curves are shown in Figure 18. It can be seen that reducing i_q indeed enhances the speed range. But in this way the torque is reduced and the power is also reduced, which indicates that only reducing i_q is not a good way.

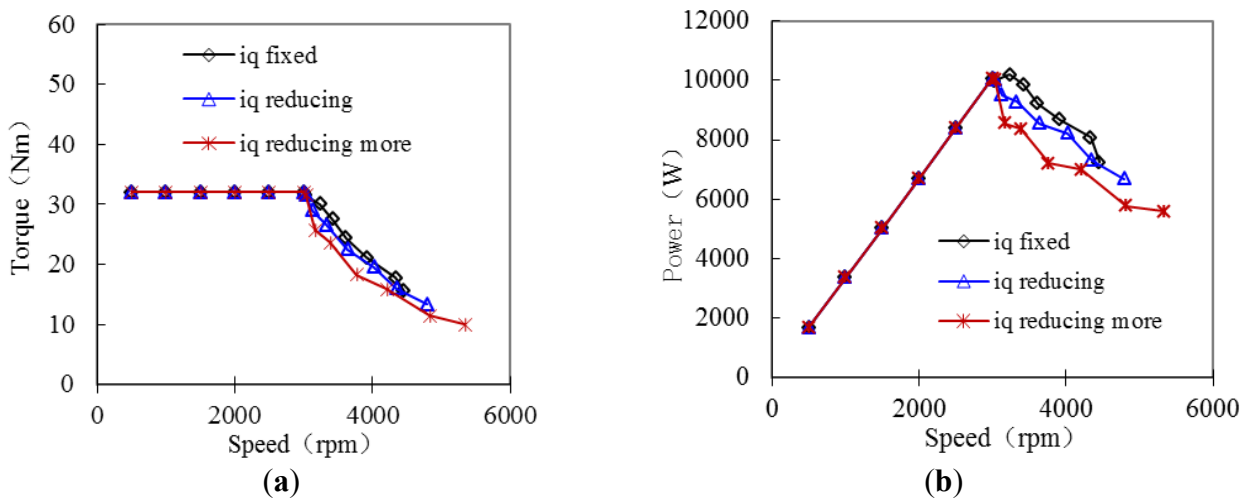


Figure 18. Field weakening results with only i_q existing: (a) torque-speed and (b) power-speed.

However, if the mechanical method of sliding PMs is combined with the electrical method of increasing d -axis current and decreasing q -axis current while keeping the total current no more than rated current, the field weakening result will be different. In this way the electromagnetic power P_{em} can be calculated based on Equations (1) and (10) as

$$P_{em} = p\psi_f i_q u_{lim} / \sqrt{(L_q i_q)^2 + (L_d i_d + \psi_f)^2} \tag{12}$$

According to Equation (12), adjusting d -axis current i_d and q -axis current i_q carefully, combined with a reduced flux linkage ψ_f , it is possible to keep the power constant above the base speed. A group of armature currents matching different sliding distance are carefully chosen based on Equations (1), (10) and (12) to keep the power as constant as possible. The armature root mean square (RMS) current above base speed is shown in Table 2. When the PMs slide to 33 mm, the PMs are prevented by the end frame and will not slide outward further with the speed increasing. Then the i_d is also unchanged. Figure 19 shows the field weakening capability with mechanical method and adjusting i_d and i_q while keeping the current amplitude no more than rated current. From the Figure 19, it can be seen that the speed range and constant power range are very wide, up to ten times of the base speed. Very satisfying field weakening capability is achieved by optimized matching the mechanical method and electrical method.

Table 2. The armature root mean square (RMS) current above base speed.

Sliding distance (mm)	i_q (A)	i_d (A)	i (A)
0	33.00	0.00	33.00
5	32.998	0.43	33.00
10	32.94	2.02	33.00
15	32.75	4.05	33.00
20	32.12	7.57	33.00
25	31.43	10.05	33.00
30	26.36	19.86	33.00
32	21.38	25.14	33.00
33	15.20	29.29	33.00
33	13.44	29.29	32.22
33	12.02	29.29	31.66
33	10.61	29.29	31.15
33	9.76	29.29	30.87
33	8.84	29.29	30.59
33	7.07	29.29	30.13
33	5.66	29.29	29.83

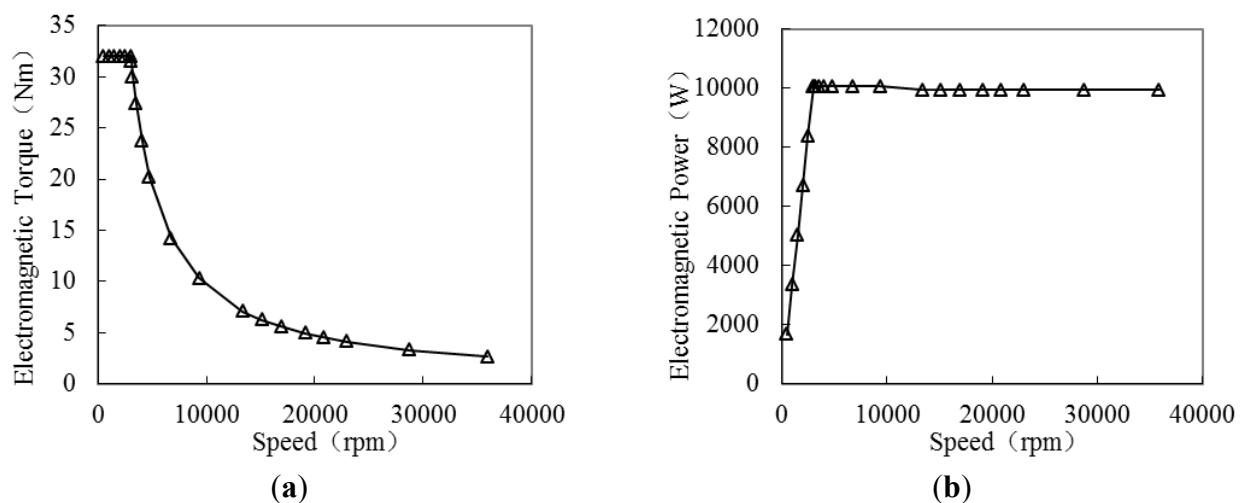


Figure 19. Field weakening capability with combination of mechanical and adjusting i_d and i_q : (a) torque-speed and (b) power-speed.

6. Force on PMs and Its influence on the performance of the machine

All the analyses above are based on the ideal position of the PMs. In order to make the PMs slide to the ideal position at different speed, it is necessary to analyze the force on the PMs while the machine is running.

6.1. Analysis of Force on PMs

Assuming that the machine runs at a certain speed, the centrifugal force F of each PM is expressed as

$$F = mr\Omega^2 \quad (13)$$

where m is the mass of the PM, r is the radius, and Ω is the mechanical angular velocity.

Based on the research in Section 5, when different currents match a PM position, the maximal speed at this position are different. So the current must be settled first. Taking the rated current all applied to the q axis during the whole process for example, the forces on the PMs are analyzed in this section.

According to the relationship between the speed and the PMs sliding distance shown in Figure 16, the relationship between centrifugal force and the sliding distance is shown in Figure 20.

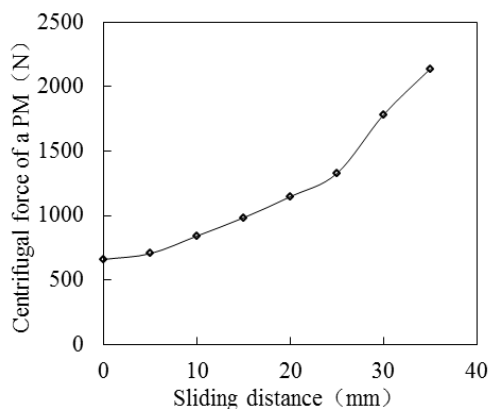


Figure 20. Relationship between centrifugal force and the sliding distance.

By calculation, the gravity force of the PM is only 0.0993% of the centrifugal force at 0 mm distance, which can be ignored here. When the machine speed is above base speed, three forces, *i.e.*, the radial electromagnetic force F_{radial} , the friction F_{μ} , and the spring force F_{spring} overcome the centrifugal force on the PMs together to ensure the PMs at ideal position.

$$F = F_{radial} + F_{\mu} + F_{spring} \quad (14)$$

The friction F_{μ} is related to the friction coefficient μ and axial electromagnetic force F_{axial} , as shown in Equation (15).

$$F_{\mu} = \mu F_{axial} \quad (15)$$

The friction coefficient is a constant value, and is assumed to be 0.2 here. The radial and axial electromagnetic force can be calculated by 3D FEM, as shown in Figure 21a. The radial force always points to the shaft center, and the value increases first and then decreases while the PMs sliding outward. The axial force always points to the rotor core and increases firstly and then changes little during the

PMs sliding outward to 33 mm. Then, the relationship between friction and the sliding distance can be obtained based on Equation (15), as shown in Figure 21b.

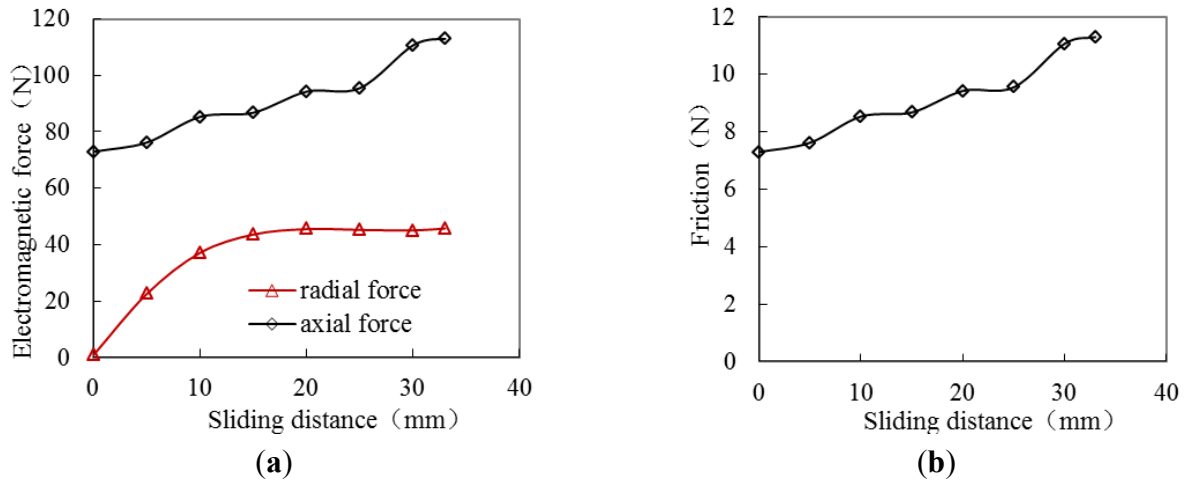


Figure 21. Relationship between electromagnetic force and friction and PMs sliding distance: (a) electromagnetic force, (b) friction.

The spring force is

$$F_{spring} = F - F_{radial} - F_{\mu} \tag{16}$$

The spring force calculated by Equation (16) is shown in Figure 22, which provides reference for choosing the suitable spring.

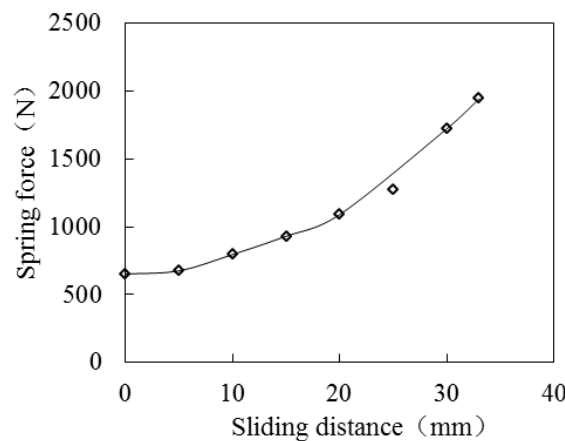


Figure 22. Relationship between spring force and PMs sliding distance.

6.2. Influence of the Friction

The PMs position keeps constant below the base speed. Above the base speed, the PMs start to slide outward during the speed increasing, and the friction on the PMs points to the center. The centripetal force provided during the speed increasing F_1 is:

$$F_1 = F_{radial} + F_{\mu} + F_{spring} = mr\Omega_1^2 \tag{17}$$

where Ω_1 is the mechanical angular velocity during speed increasing.

However, during the speed decreasing, the PMs slide inward, and the friction on the PMs is opposite to the center. The centripetal force provided during the speed decreasing F_2 is:

$$F_2 = F_{radial} - F_{\mu} + F_{spring} = mr\Omega_2^2 \tag{18}$$

where Ω_2 is the mechanical angular velocity during speed decreasing.

Because the directions of the frictions during speed increasing and decreasing are opposite, the centripetal force provided during speed increasing is higher than that during speed increasing, *i.e.*

$$F_1 > F_2 \tag{19}$$

So for the same sliding distance, the speed during speed increasing is higher than during speed decreasing, *i.e.*

$$\Omega_1 > \Omega_2 \tag{20}$$

According to Equations (17) and (18), the speed difference between speed increasing and speed decreasing is:

$$\Omega_1 - \Omega_2 = \sqrt{2F_{\mu} / mr} \tag{21}$$

From Equation (21), it can be seen that the higher the friction is, the bigger the speed difference is. Because of this speed difference, the relationships between the electromagnetic parameters and the speed show a hysteretic characteristic, which means the trace during speed increasing is not the same with the trace during speed decreasing. In order to make this phenomenon more obvious, a larger friction coefficient $\mu = 1$ is also considered.

Figure 23 shows the relationship of flux linkage *versus* speed. Figure 24 shows the relationship of back EMFs *versus* speed. Figure 25 shows the relationship of average torque *versus* speed. From Figures 23–25, it can be seen that all the curves show hysteretic characteristics. The higher the friction coefficient is, the more obvious the hysteretic characteristic is, which is in agreement with the analysis. The torque output ability is reduced during speed decreasing. The no-load and load EMFs during speed decreasing are all smaller than that during speed increasing. So some rules must be followed to design this type of PMSM: the EMF should be designed at speed increasing process to ensure the EMF smaller than the terminal voltage of the machine. The friction coefficient must be as small as possible to reduce the hysteretic characteristic.

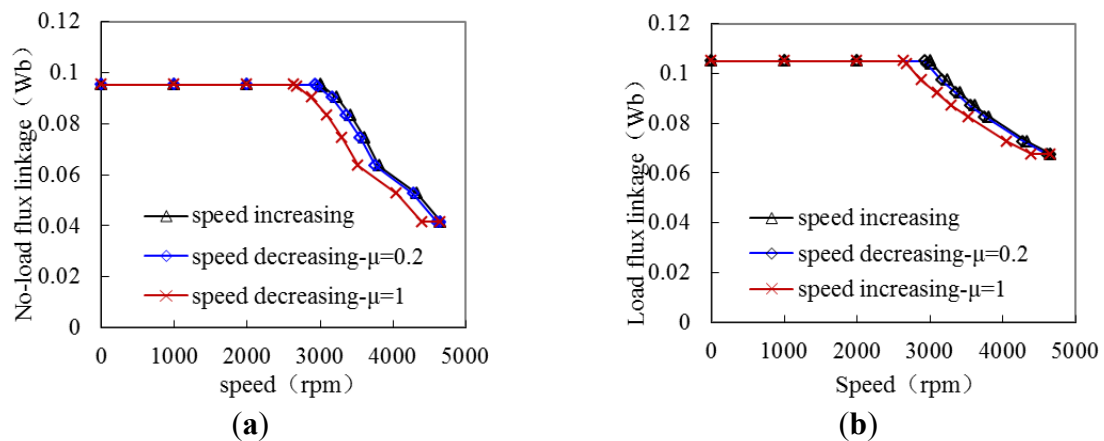


Figure 23. Relationship of flux linkage *versus* speed: (a) no-load flux linkage, (b) load flux linkage.

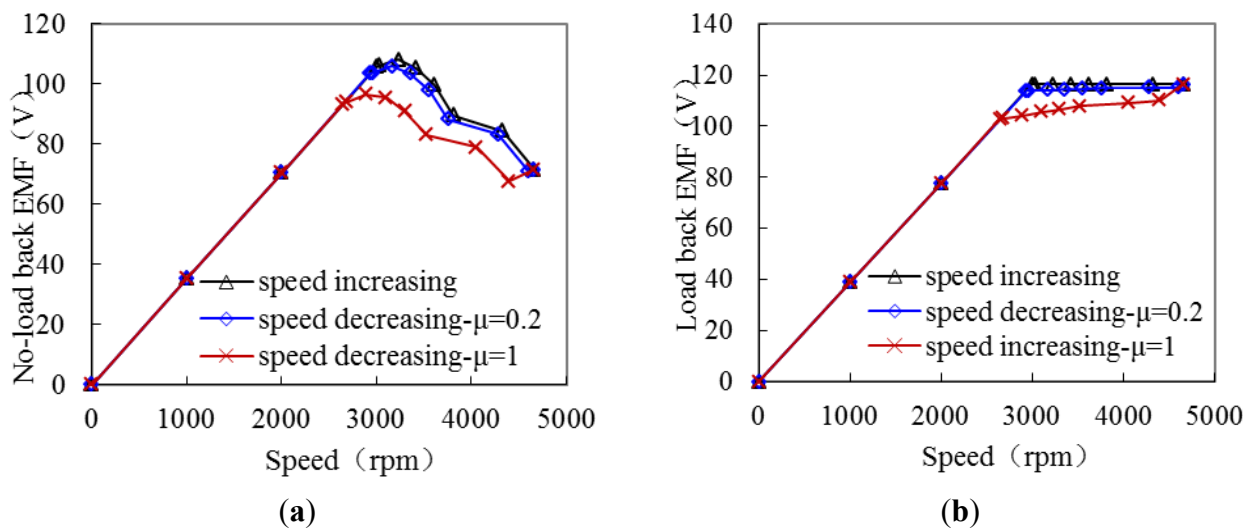


Figure 24. Relationship of back EMF *versus* speed: (a) no-load back EMF; (b) load back EMF.

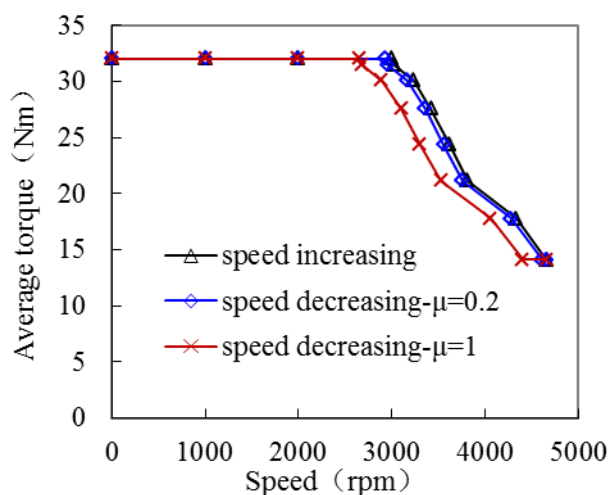


Figure 25. Relationship of average torque *versus* speed.

7. Conclusions

An axial flux PMSM with radially sliding PMs to fulfill field-weakening control by mechanical method is investigated in this paper. The field weakening principle and the structure of this kind of axial flux PMSM are introduced and analyzed. The influences of radially sliding PMs on magnetic flux density distribution are analyzed based on 3D FEM. It is found that the magnetic flux density distribution in stator iron is different from that in air gap due to the 3D equal permeability. The changing laws of d - and q -axis inductances with sliding distance are analyzed and discussed based on magnetic circuit and FEM calculation. The influences of radially sliding PMs on flux linkage and torque are also analyzed and evaluated.

The field weakening effects by the mechanical method of PMs sliding and by the electrical method of adjusting the d - and q -axis current are compared. It is found the field weakening effects by the two methods are more or less, and neither of them can provide satisfying field weakening capability independently. The combination of mechanical method and electrical method is researched. It is found that the mechanical method of PMs sliding combining only q -axis current without any d -axis current

cannot provide a satisfying field weakening effect. However, field-weakening capability of the machine can be much improved by the optimized combination of the mechanical method of PMs sliding and by adjusting the d- and q-axis current together while keeping the total current no more than rated current.

The forces on the PMs are analyzed and calculated. The radial electromagnetic force, friction and the spring force on the PM overcome the centrifugal force together to ensure the PMs at an ideal position. During speed increasing and speed decreasing above base speed, the hysteretic characteristics on flux linkage, back EMF and torque caused by the friction of the PMS are investigated, which provide useful reference for designing this kind of machine.

Acknowledgments

This work was supported in part by the National Natural Science Foundation of China under Project 50577011 and 51307008, in part by Ph.D. Programs Foundation of Ministry of Education of China under Project 20121101120024, in part by Key laboratory for Intelligent Control & Decision of Complex Systems, Beijing Institute of Technology, in part by Basic Research Foundation of Beijing Institute of Technology under Grant 20120642013 and 20130642015, and in part by Excellent Young Scholars Research Fund of Beijing Institute of Technology.

Author Contributions

All authors contributed to this work by collaboration. Jing Zhao is the main author of this manuscript. Bin Li and Zhongxin Gu provided some useful suggestions in the construction of paper.

Conflicts of Interest

The authors declare no conflict of interest.

References

1. Yang, Y.P.; Chuang, D.S. Optimal Design and Control of a Wheel Motor for Electric Passenger Cars. *IEEE Trans. Magn.* **2007**, *43*, 51–61.
2. Wang, J.B.; Yuan, X.B.; Atallah, K. Design Optimization of a Surface-Mounted Permanent-Magnet Motor with Concentrated Windings for Electric Vehicle Applications. *IEEE Trans. Veh. Technol.* **2013**, *62*, 1053–1064.
3. Zhu, Z.Q.; Howe, D. Electrical Machines and Drives for Electric, Hybrid, Fuel Cell Vehicles. *Proc. IEEE* **2007**, *95*, 746–765.
4. Yang, H.; Lin, H.Y.; Zhu, Z.Q.; Fang, S.H.; Huang, Y.K. Novel Flux-Regulatable Dual-Magnet Vernier Memory Machines for Electric Vehicle Propulsion. *IEEE Trans. Appl. Supercon.* **2014**, *24*, Article 0601205.
5. Cai, H.W.; Guan, B.; Xu, L.Y. Low-Cost Ferrite PM-Assisted Synchronous Reluctance Machine for Electric Vehicles. *IEEE Trans. Ind. Electron.* **2014**, *61*, 5741–5748.
6. Patel, V.; Wang, J.B.; Wang, W.Y.; Chen, X. Six-Phase Fractional-Slot-per-Pole-per-Phase Permanent-Magnet Machines with Low Space Harmonics for Electric Vehicle Application. *IEEE Trans. Ind. Appl.* **2014**, *50*, 2554–2563.

7. Hua, W.; Yin, X.M.; Zhang, G.; Cheng, M. Analysis of Two Novel Five-Phase Hybrid-Excitation Flux-Switching Machines for Electric Vehicles. *IEEE Trans. Magn.* **2014**, *50*, Article 8700305.
8. Xiao, F.; Deng, Q.L.; Liu, J.C. Design of Direct-Drive Axial Flux Permanent Magnet in-Wheel Machine for Electric Vehicle. In Proceedings of the International Conference on Electrical Machines and System (ICEMS), Beijing, China, 20–23 August 2011; pp. 1–4.
9. Ho, S.L.; Niu S.X.; Fu, W.N. Design and Analysis of a Novel Axial-Flux Electric Machine. *IEEE Trans. Magn.* **2011**, *47*, 4368–4371.
10. Ficheux, R.L.; Associate, L.; Caricchi, F.; Crescimbin, F.; Honorati, O. Axial-Flux Permanent-Magnet Motor for Direct-Drive Elevator Systems without Machine Room. *IEEE Trans. Ind. Appl.* **2001**, *37*, 1693–1701.
11. Nguyen, T.D.; Tseng, K.J.; Zhang, S.; Nguyen, H.T. A Novel Axial Flux Permanent Magnet Machine for Flywheel Energy Storage System: Design and Analysis. *IEEE Trans. Ind. Electron.* **2011**, *58*, 3784–3794.
12. Gerlando, A.D.; Foglia, G.M.; Iacchetti, M.F.; Perini, R. Effects of Manufacturing Imperfections in Concentrated Coil Axial Flux PM Machines: Evaluation and Tests. *IEEE Trans. Ind. Electron.* **2014**, *61*, 5012–5024.
13. Iafari-Shiadeh, S.M.; Ardebili, M. Analysis and Comparison of Axial-Flux Permanent-Magnet Brushless-DC Machines with Fractional-Slot Concentrated-Windings. In Proceedings of the Power Electronics, Drive Systems and Technologies Conference (PEDSTC), Tehran, Iran, 13–14 February 2013; pp. 72–77.
14. Winter, O.; Kraland, C.; Schmidt, E. Design and Loss Assessment of Air Cored Axial Flux Permanent Magnet Machines. In Proceedings of the IEEE International Electric Machines & Drives Conference (IEMDC), Chicago, IL, USA, 12–15 May 2013; pp. 602–606.
15. Eastham, J.F.; Profumo, F.; Tenconi, A.; Hill-Cottingham, R.; Coles, P.; Gianolio, G. Novel Axial Flux Machine for Aircraft Drive: Design and Modeling. *IEEE Trans. Magn.* **2002**, *38*, 3003–3005.
16. Stefano, R.D.; Marignetti, F. Electromagnetic Analysis of Axial-Flux Permanent Magnet Synchronous Machines with Fractional Windings with Experimental Validation. *IEEE Trans. Ind. Electron.* **2012**, *59*, 2573–2582.
17. Upadhyay, P.R.; Rajagopal, K.R.; Singh, B.P. Design of a Compact Winding for an Axial-Flux Permanent-Magnet Brushless DC Motor Used in an Electric Two-Wheeler. *IEEE Trans. Magn.* **2004**, *40*, 2026–2028.
18. Yang, Y.P.; Liang, J.Y.; Xing, X.Y. Design and Application of Axial-Flux Permanent Magnet Wheel Motors for an Electric Vehicle. In Proceedings of the AFRICON 09, Nairobi, Kenya, 23–25 September 2009; pp. 1–5.
19. Lee, C.H.T.; Liu, C.H.; Chau, K.T. A Magnetless Axial-Flux Machine for Range-Extended Electric Vehicles. *Energies* **2014**, *7*, 1483–1499.
20. Tang, R. *Modern Permanent Magnet Machines-Theory and Design*, 1st ed.; China Machine Press: Beijing, China, 2012; pp. 38–48, 244–263.
21. Gonzalez-Lopez, D.A.; Tapia, J.A.; Wallace, R.; Valenzuela, A. Design and Test of an Axial Flux Permanent-Magnet Machine With Field Control Capability. *IEEE Trans. Magn.* **2008**, *44*, 2168–2173.

22. Kwon, T.S.; Sul, S.K.; Alberti, L.; Bianchi, N. Design and Control of an Axial-Flux Machine for a Wide Flux-Weakening Operation Region. *IEEE Trans. Ind. Appl.* **2009**, *45*, 1258–1266.
23. Aydin, M.; Huang, S.; Lipo, T.A. A New Axial Flux Surface Mounted Permanent Magnet Machine Capable of Field Control. *IEEE Ind. Appl. Conf.* **2002**, *2*, 1250–1257.
24. Aydin, M.; Huang, S.; Lipo, T.A. Design, Analysis, and Control of a Hybrid Field-Controlled Axial-Flux Permanent-Magnet Motor. *IEEE Trans. Ind. Electron.* **2010**, *57*, 78–87.
25. Ferraro, L.D.; Caricchi, F.; Capponi, F.G. Analysis and Comparison of a Speed-Dependant and a Torque-Dependant Mechanical Device for Wide Constant Power Speed Range in AFPM Starter/Alternators. *IEEE Trans. Power Electron.* **2006**, *21*, 720–729.
26. Oh, S.C.; Emadi, A. Test and Simulation of Axial Flux-Motor Characteristics for Hybrid Electric Vehicles. *IEEE Trans. Veh. Technol.* **2004**, *53*, 912–919.
27. Kober, W.; Fairport, N.Y. Electric Generator and Regulator. U.S. Patent 2824275, 18 February 1958.
28. Zhao, J.; Yan, Y.S.; Gu, Z.X.; Chen, Z.; Zheng, P. Research on an Axial-Axial Flux Compound-Structure PMSM with Varying Air Gap to Fulfill Field-Weakening Control. In Proceedings of the Electrical Machines and Systems, Hangzhou, China, 22–25 October 2014; pp. 3345–3349.
29. Rao, D.K. Axial Gap Motor with Radially Movable Magnets to Increase Speed Capability. U.S. Patent 6194802, 27 February 2001.
30. Zhao, J.; Cheng, D.S.; Zheng, P.; Liu, X.D.; Tong, C.D.; Song, Z.Y.; Zhang, L. Field Weakening Capability Investigation of an Axial Flux PMSM with Radially Sliding Permanent Magnets Used for Electric Vehicles. *J. Appl. Phys.* **2012**, doi:10.1063/1.3676230.
31. Chun, Y.D.; Koo, D.-H.; Cho, Y.-H.; Cho, W.-Y. Cogging Torque Reduction in a Novel Axial Flux PM Motor. In Proceedings of the International Symposium on Power Electronics, Electrical Drives, Automation and Motion, Taormina, Italy, 23–26 May 2006; pp. 1020–1023.
32. Enomoto, Y. Evaluation of Experimental Permanent-Magnet Brushless Motor Utilizing New Magnetic Material for Stator Core Teeth. *IEEE Trans. Magn.* **2005**, *41*, 4304–4308.
33. Wang, J.B.; Howe, D. Influence of Soft Magnetic Materials on the Design and Performance of Tubular Permanent Magnet Machines. *IEEE Trans. Magn.* **2005**, *41*, 4057–4059.
34. Chen, Y.S.; Zhu, Z.Q.; Howe, D. Calculation of d - and q -Axis Inductances of PM Brushless ac Machines Accounting for Skew. *IEEE Trans. Magn.* **2005**, *41*, 3940–3942.